Materials Research. 2013; 16(6): 1229-1236
DOI: 10.1590/S1516-14392013005000129

Effect of Cooling Rate on (ε, α') Martensite Formation in Twinning/transformation-induced Plasticity Fe–17Mn–0.06C Steel

Sara Silva Ferreira de Dafé, Felipe Lucas Sicupira, Flávia Cristina Silva Matos, Naiara Silva Cruz,

Débora Rezende Moreira, Dagoberto Brandão Santos*

Department of Metallurgical and Materials Engineering, Escola de Engenharia, Universidade Federal de Minas Gerais – UFMG, Bloco 2, Av. Antônio Carlos, 6627, Pampulha, CEP 31270-901, Belo Horizonte, MG, Brazil

Received: November 16, 2012; Revised: April 7, 2013

The cooling rate, density of stacking faults, austenite grain size, and temperature strongly influence the $\gamma_{fcc} \rightarrow \varepsilon_{hcp} \rightarrow \alpha'_{bcc}$ martensite transformation in austenitic alloys. During cooling, austenitic Fe–Mn steels can partially transform to ε and α' martensites within a restricted chemical composition. Martensite formation will influence the mechanical behavior of the alloy. The microstructure evolution under three cooling rates of a hot-rolled austenitic steel, Fe–17.0Mn–0.06C (wt%), was analyzed by optical microscopy and scanning electron microscopy/electron backscatter diffraction. The volume fraction of martensite and austenite were measured by X-ray diffraction line profile analysis by directly comparing the as-cast alloy, alloy subjected to different cooling conditions, and this processed with hot rolling.

Keywords: *cooling rate; martensite formation; grain boundaries; stacking fault energy.*

1. Introduction

Fe–C–Mn–Al–Si alloys have attracted significant interest in physical metallurgy and materials science because their mechanical properties such as high ductility and strength are important for industries[1-5]. Steels with high Mn content (15-30%) and alloy elements Si and Al have high strength and exceptional plasticity owing to either twinning-induced plasticity (TWIP) or the transformation-induced plasticity (TRIP) that results from multiple martensitic transformations such as γ_{fcc} (austenite) $\rightarrow \varepsilon_{hcp}$ (hcp-martensite) $\rightarrow \alpha'_{bcc}$ (bcc-martensite)[5-8].

For twinning to occur, it is usually necessary for the steel stacking fault energy (SFE) to be in the range of 18-35 mJ/m^2. If the SFE is <18 mJ/m^2, twinning is replaced by martensitic transformation. However, if it is >35 mJ/m^2, then the slipping processing will be the only mechanism that contributes to the plastic deformation of steel[9,10].

The stability of austenite in these steels is of great importance because of the phase transformation that accompanies the plastic deformation that occurs either through twinning or martensitic transformation. The latter depends on the steel chemical composition, temperature, austenite grain size, and amount of stress applied to the steel. The formation of martensite can be induced thermally or by applying strain[10-14]. During cooling, the austenitic Fe–Mn steel, within a restricted range of chemical composition, partially transforms into ε_{hcp} and α'_{bcc} martensite, while retaining some the untransformed austenite[12-15].

Stacking faults and twinning are important for the formation of martensite in Fe–Mn–Si–Al steels because they act as nucleation sites for martensite formation[16-19]. The fcc-phase transformation $\gamma \rightarrow \varepsilon_{hcp}$ occurs through the formation of alternate layers of stacking faults in the (111) planes of austenite. α' martensite is formed either directly from austenite or at the intersections of different variants of ε martensite[8,9,20].

In addition to the cooling rate and crystallographic defects, the prior austenite grain size (PAGS) is another parameter that controls the stability of the austenite, because the formation of martensite can be prevented by the presence of a large numbers of barriers in the microstructure, such as twin or grain boundaries and deformation defects[11,12,14].

The industrial production of TRIP and TWIP steels always involves thermo-mechanical processing such as hot rolling, cold rolling at room temperature, and annealing. In all these stages, the steel goes through thermal cycles involving both heating and cooling. However, research has tended to focus on the martensitic transformation from deformed structures[2-4,9,10,15]. Few studies have considered the formation of martensite in TRIP and TWIP steels in the absence of strain. Only those transformations resulting from cooling, or the reversal of martensite to austenite in alloys that exhibit the shape memory effect, have been considered[11-13,19,20].

This study evaluates the effect of large austenitic grain size and the variation of cooling rate on the formation of ε and α' martensite in a steel with 17% Mn and 0.06% C. TWIP steels with similar Mn content but much higher carbon content (0.2-0.6% C) have been analyzed in previous reports[7,10,12,15,21]. However, the chemical composition of

*e-mail: dsantos@demet.ufmg.br

the steel discussed in this study has not been reported in the literature yet. This chemical composition provides the steel a low SFE, thereby greatly facilitating the formation of martensite[8]. Therefore, we need to increase our knowledge of the physical characteristics of these alloys in order to better understand the stability of austenite during their industrial processing.

2. Experimental Procedure

In this study, TRIP/TWIP steel was utilized and its composition is listed in Table 1. The steel was melted in Keel ASTM A370 block form by air in an induction furnace (Power Trak 250-10 R Inductotherm®). The steel was melted and cast at 1558 °C and 1510 °C, respectively. Plates were removed from the Keel blocks, austenitized at 1100 °C for 2 h, and then cooled in water to homogenize their microstructure and chemical composition. After homogenization, samples were cut for hot rolling, which performed at 1070 °C with four passes of equal reduction leading to a total thickness reduction of 50%. The resulting thickness was 12.0 mm.

From the hot-rolled sheet, a 100 × 20 × 12 mm sample was divided into three equal parts, which were then heated at 1000 °C for 3600 s. After soaking, three different cooling methods were applied: natural air (AS), immersion in water (WS), and inside the furnace after its shutdown (FS). The samples were also examined in the as-cast and hotrolled conditions. After the heat treatment, they were divided into two parts. One part was hot-mounted for metallographic examination while the other was used for X-ray diffraction (XRD) analysis. All the samples were carefully conventionally ground and polished with 0.25- mm diamond paste. Their microstructure was analyzed via optical and scanning electron microscopy (SEM), etched initially with 4% Nital. The grain size was measured using the software Image Pro Plus®. Electron backscatter diffraction (EBSD) analysis was also carried out to study the crystallography of the phase transformation, for which the samples were additionally polished with colloidal silica (size 0.02 mm) before the final examination.

The retained austenite and the ε and α′ martensite volume fractions were quantified by XRD with Cu Kα radiation via the direct comparison method[22]. This method uses the integration of the most intensive peaks of (i) austenite, characterized by the (111), (200), (220), and (311) planes; (ii) α' martensite, characterized by the (110), (200), (211), and (220) planes; and (iii) ε martensite, characterized by the (100), (002), (101), and (102) planes. We used the Origin™ software for integrating these peaks with a peak-fitting tool.

Table 1. Chemical composition of TRIP/TWIP[a] steel.

Element	Mn	Al	Si	Ni	C
Mass%	17.0	3.0	2.0	1.0	0.06

[a]TWIP, twinning-induced plasticity; TRIP, transformation-induced plasticity.

3. Results and Discussion

3.1. *Stacking fault energy*

The addition of alloying elements such as Al and Ni increases the SFE and tends to inhibit the martensitic transformation (γ→ ε →α'), whereas the addition of Si decreases the SFE, thereby favoring the formation of martensite during cooling and deformation.The SFE (Γ) in TRIP/TWIP steel can be estimated using the model proposed by Dumay et al.,[18] according to Equation 1[23]:

$$\Gamma = 2\rho\Delta G^{\gamma\to\varepsilon} + 2\sigma^{\gamma/\varepsilon} \quad (1)$$

Where ρ is the molar surface density of atoms in the plane {111} and equal to $2.94*10^{-5}$ mol.m^{-2}, $\Delta G^{\gamma\to\varepsilon}$ is the molar Gibbs free energy of transformation γ→ε, and $\sigma^{\gamma\to\varepsilon}$ is the surface energy associated with the interface between the γ and ε phases and corresponds to 8 mJm^{-2}.

The free energy of martensite formation can be represented by Equation 2:

$$\Delta G^{\gamma\to\varepsilon} = \Delta G^{\gamma\to\varepsilon}_{FeMnX} + x_c\Delta G^{\gamma\to\varepsilon}_{FeMnX/C} + \Delta G^{\gamma\to\varepsilon}_{mg} \quad (2)$$

$\Delta G^{\gamma\to\varepsilon}_{FeMnX}$ is the contribution of the substitutional chemical elements in CFC lattice phase. The terms in excess of Fe, Mn, Si, Al and Ni are considered in this calculation, but other elements are neglected due to the low level in this alloy. This contribution is shown in Equation 3:

$$\Delta G^{\gamma\to\varepsilon}_{FeMnX} = \sum_i x_i\Delta G_i^{\gamma\to\varepsilon} + x_{Fe}x_{Mn}[C + D(x_{Fe} - x_{Mn})] + x_{Fe}x_{Si}[E + F(x_{Fe} - x_{Si})] \quad (3)$$

Where: *xi* is the mole fraction of each element, T is temperature and C, D, E and F are adjusted values.

The effect of the carbon content in combination with the manganese content is given by Equation 4, where a, b and c are adjusted values.

$$\Delta G^{\gamma\to\varepsilon}_{FeMnX/C} = \frac{a}{x_c}(1 - e^{-bx_c}) + cx_{Mn} \quad (4)$$

$\Delta G^{\gamma\to\varepsilon}_{mg}$ is a term due to Néel magnetic transition, which corresponds to the phase transformation of the paramagnetic phase to the antiferromagnetic γ and ε.

$$\Delta G^{\gamma\to\varepsilon}_{mg} = G^{\varepsilon}_m + G^{\gamma}_m \quad (5)$$

Where:

$$G^{\varphi}_m = RT\ln\left(1 + \frac{\beta^{\varphi}}{\mu_B}\right) * f\left(\frac{T}{T^{\varphi}_N}\right), \varphi \text{ are the phases } \gamma \text{ e } \varepsilon \quad (6)$$

Since the magnetic moment, β^{φ}, (Equation 8), T^{φ}_N the Néel temperature, μ_B, the Bohr magneton and *f* is a function given by Equation 7:

$$f^{\varphi}(\tau^{\varphi}) = \frac{-1}{2{,}34}\left[\frac{\tau^{-5}}{10} + \frac{\tau^{-15}}{315} + \frac{\tau^{-25}}{1500}\right], \tau = \left(\frac{T}{T^{\varphi}_N}\right) > 1 \quad (7)$$

$$\beta^{\gamma} = \beta^{\gamma}_{Fe}x_{Fe} + \beta^{\gamma}_{Mn}x_{Mn} - \beta^{\gamma}_{FeMn}x_{Fe}x_{Mn} - \beta^{\gamma}_{C}x_{C} \quad (8a)$$

$$\beta^{\varepsilon} = \beta^{\varepsilon}_{Mn}x_{Mn} - \beta^{\varepsilon}_{C}x_{C} \quad (8b)$$

Where β_i^{φ} is the contribution of the element *i* in phase φ and β_{ij}^{φ} is the term in excess. The Néel temperature for the different phases is given by Equation 9a, b:

$$T_N^{\gamma} = 250\ln(x_{Mn}) - 4750x_c x_{Mn} - 222x_{Cu} - 2{,}6x_{Cr} - 6{,}2x_{Al} - 13x_{Si} + 720 \quad \text{(K) (9a)}$$

$$T_N^{\varepsilon} = 580x_{Mn} \quad \text{(K) (9b)}$$

The values required for the calculation of the SFE are shown in Table 2. Using an electronic spreadsheet, the calculated value of the SFE for steel in this work is 14.5 mJ/m^2.

3.2. *Analysis by X-ray diffraction*

Figure 1 shows the XRD patterns of samples subjected to the three different cooling rates and those of the as-cast and hot-rolled conditions. The coexistence of austenitic and martensitic phases in the samples can be confirmed by their respective peaks in the diffraction patterns, the EBSD images shown in Figure 2, and the results in Table 3.

Table 2. Summary of the parameters used in the model of Dumay et al.[18].

$\Delta G_{Fe}^{\gamma\to\varepsilon}$	–2243,38 + 4,309T (Jmol^{-1})
$\Delta G_{Mn}^{\gamma\to\varepsilon}$	–1000 + 1.123T (Jmol^{-1})
$\Delta G_{FeMn}^{\gamma\to\varepsilon}$	C = 2873 Jmol^{-1}, D =–717 Jmol^{-1}
$\Delta G_{FeMnX/C}^{\gamma\to\varepsilon}$	a = 1246 Jmol^{-1}, b = 24,29 Jmol^{-1}, c = –17175 Jmol^{-1}
$\frac{\beta^{\gamma}}{\mu_B}$	$0{,}7x_{Fe} + 0{,}62x_{Mn} - 0{,}64x_{Fe}\,x_{Mn} - 4x_C$
$\frac{\beta^{\varepsilon}}{\mu_B}$	$0{,}62x_{Mn} - 4\,x_C$
$\Delta G_{Al}^{\gamma\to\varepsilon}$	2800 + 5T (Jmol^{-1})
$\Delta G_{Si}^{\gamma\to\varepsilon}$	-560 – 8T (Jmol^{-1})
$\Delta G_{FeSi}^{\gamma\to\varepsilon}$	E= 2850 J mol^{-1}, F = 3520 Jmol^{-1}
$\Delta G_{Ni}^{\gamma\to\varepsilon}$	1423 Jmol^{-1} [5]

The ε-martensite-starting temperature ($M\varepsilon_s$) gradually decreases with increasing Mn content and alloy elements. Equation 10, derived from the multiple regression analysis by Yang et al.,[24] provides $M\varepsilon_s$ value for the steel used in present work as 174 °C. Coincidentally, $M\varepsilon_s$ reported by Tsuzaki et al.[25] for 16Mn–0.006C steel was also 174 °C. ε martensite transforms from austenite before α' martensite does. However, no relation was found in the literature for calculating $M\alpha'_s$ after ε martensite formation.

$$M\varepsilon_s\ (K) = 576 - 489(\%C) - 9.1(\%Mn) - 17.6(\%Ni) - 9.2(\%Cr) + 21.3(\%Al) + 4.1(\%Si) - 19.4(\%Mo) - 1(\%Co) - 41.3(\%Cu) - 50(\%Nb) - 86(\%Ti) - 4(\%V) - 13(\%W) \quad (10)$$

The ε and α' martensite transformations occur in the steel used in the present work because of different cooling rates, mainly in an athermal mode, assisted by some strain resulting from solidification or thermal contraction. However, it was not possible to separate the amount of each transformation.

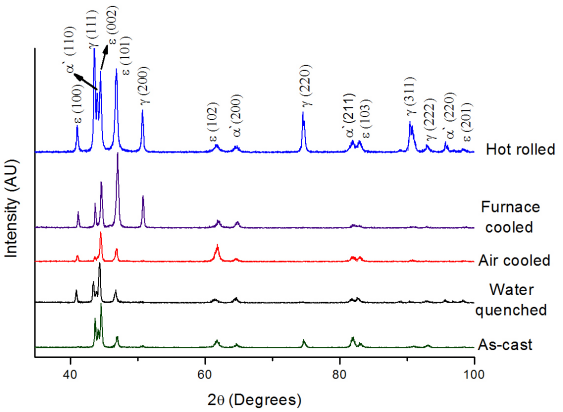

Figure 1. X-ray diffractograms after different processing conditions of the steel.

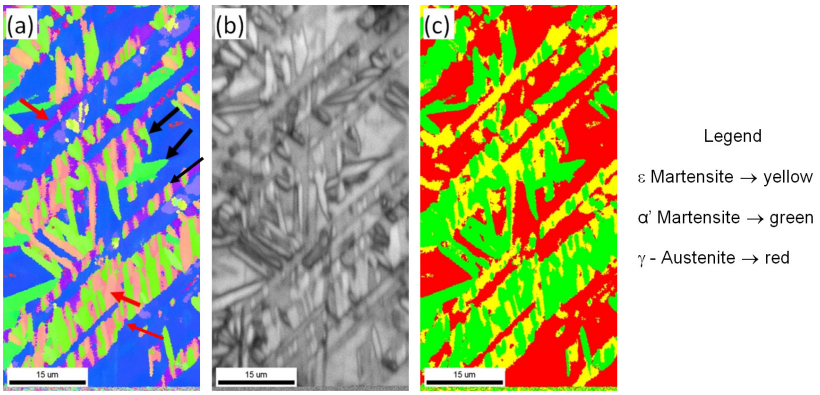

Figure 2. EBSD evaluation. (a) IPF (inverse pole figure), (b) IQ (image quality) map, and (c) phase map for the samples annealed at 1000 °C for 1 h and furnace cooled.

In the as-cast sample, despite the slow cooling during the thermal cycle, residual stress generated because of the contraction during the solidification of the alloy. These stresses can result into a larger volume fraction of ε and α' martensite.

The same reasoning is applied to the WS sample. In this case, the stress was owing to thermal contraction[11]. For the FS sample, the steel is subjected to a high temperature for a longer period of time, which allows stress relief, resulting in a lower volume fraction of α' martensite and greater stabilization of austenite. On the other hand, the AS sample led to a greater fraction of ε martensite (Table 3).

According to Sahu et al.,[15] the increase in the volume fraction of ε martensite would be justified because of its isothermally transformed amount. The phase-transformation kinetics would be favored by a longer cooling time in air in relation to the cooling carried out in water. Because the cooling in air and in the furnace are continuous and slow processes, they would favor the formation of isothermal martensite during cooling from temperatures higher than $M\varepsilon_s$. It is expected that α′ martensite formed during cooling in water will be athermal and dependent only on the temperature, whereas the amount of isothermal martensite depends on both the temperature and the time.

3.3. *Metallographic characterization*

3.3.1. EBSD analysis

Figure 2 shows the EBSD results of the sample annealed at 1000 °C for 1 h and furnace cooled.

Table 3. Phase volume fractions of samples measured by X-ray diffraction.

Sample	Volume fraction (%)		
	ε	α'	γ
As-cast	50.4	26.1	23.6
Furnace cooled	70.6	7.9	21.5
Air cooled	78.1	16.6	5.5
Water quenched	60.4	20.6	18.8
Hot rolling	41.7	15.8	42.5

Verbeken et al.[20] demonstrated that although the specific nature of the austenite to ε martensite transformation is still in question, EBSD has a high potential for identifying ε martensite. In Figure 2a, the black arrows indicate α' martensite, whereas the red arrows show ε martensite; the blue background is austenite in different orientations. In the annealed specimen, the austenite grain boundaries are not delineated because of the high magnification used in the EBSD image. Figure 2b shows a phase-contour delineation of the microstructure inside the austenitic grains, where different crystallographic variants of α' and ε martensite coexist.

Figure 2c shows a strong interaction between α' and ε martensite. There is no α' martensite that is unassociated with ε martensite. This observation highlights the fact that α' is being formed from ε and not directly from the austenite in the steel under study. The lenticular and bulk morphologies of α' are well defined, as indicated in Figure 2a by the black arrows. One difficulty indicated by Verbeken et al.[20] in evaluating austenite and ε martensite phases by EBSD is because of the close proximity of each unit. As long as ε martensite is formed as extremely fine plates[9,26] resulting from twinning, some austenite is invariably left between the plates, leading to increased difficulty in obtaining Kikuchi indexing lines. Quantitatively, it can also lead to a lower image quality (IQ) index, as seen in Figure 2b, assessed by the system software.

3.3.2. Optical and SEM metallography

As-cast and heat-treated structures

Figures 3-5 show the optical and scanning electron micrographs of the as-cast samples and under the three cooling conditions: water, air, and furnace. PAGS reached a wide range of 200-1000 μm, as seen in Figure 5.

Figures 4a and 4b show that α' martensite grew in different directions. This certainly is because of continuous nucleation and growth. Although the growth rate can be fast, in order to reach the M_{ef} (ε martensite finish temperature), α' martensite must nucleate in the ε martensite plates because they are formed during the cooling process.

Figures 4a and 4d show that ε martensite is formed within the austenitic grain, which then spreads until it reaches the opposite grain boundary where the orientation of

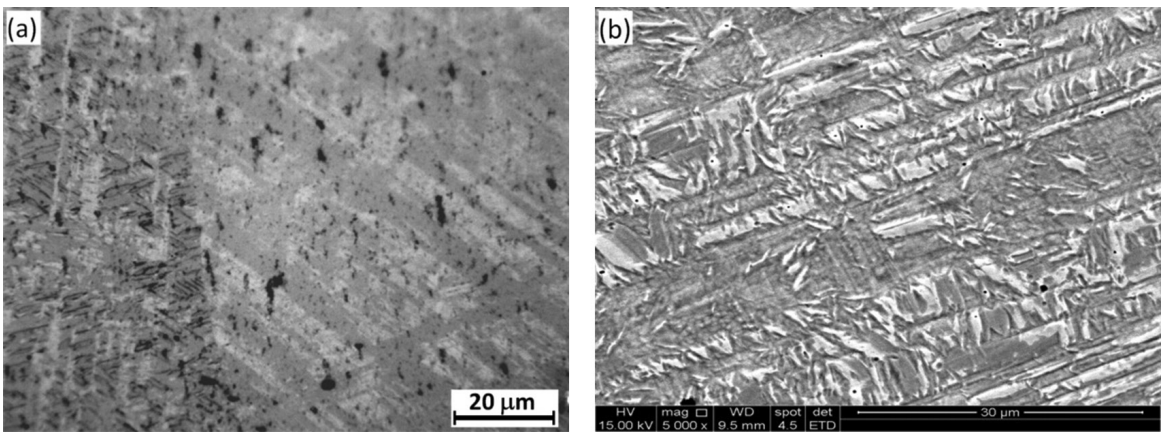

Figure 3. (a) Optical and (b) scanning electron micrographs of the as-cast sample. Samples were etched with 4% Nital.

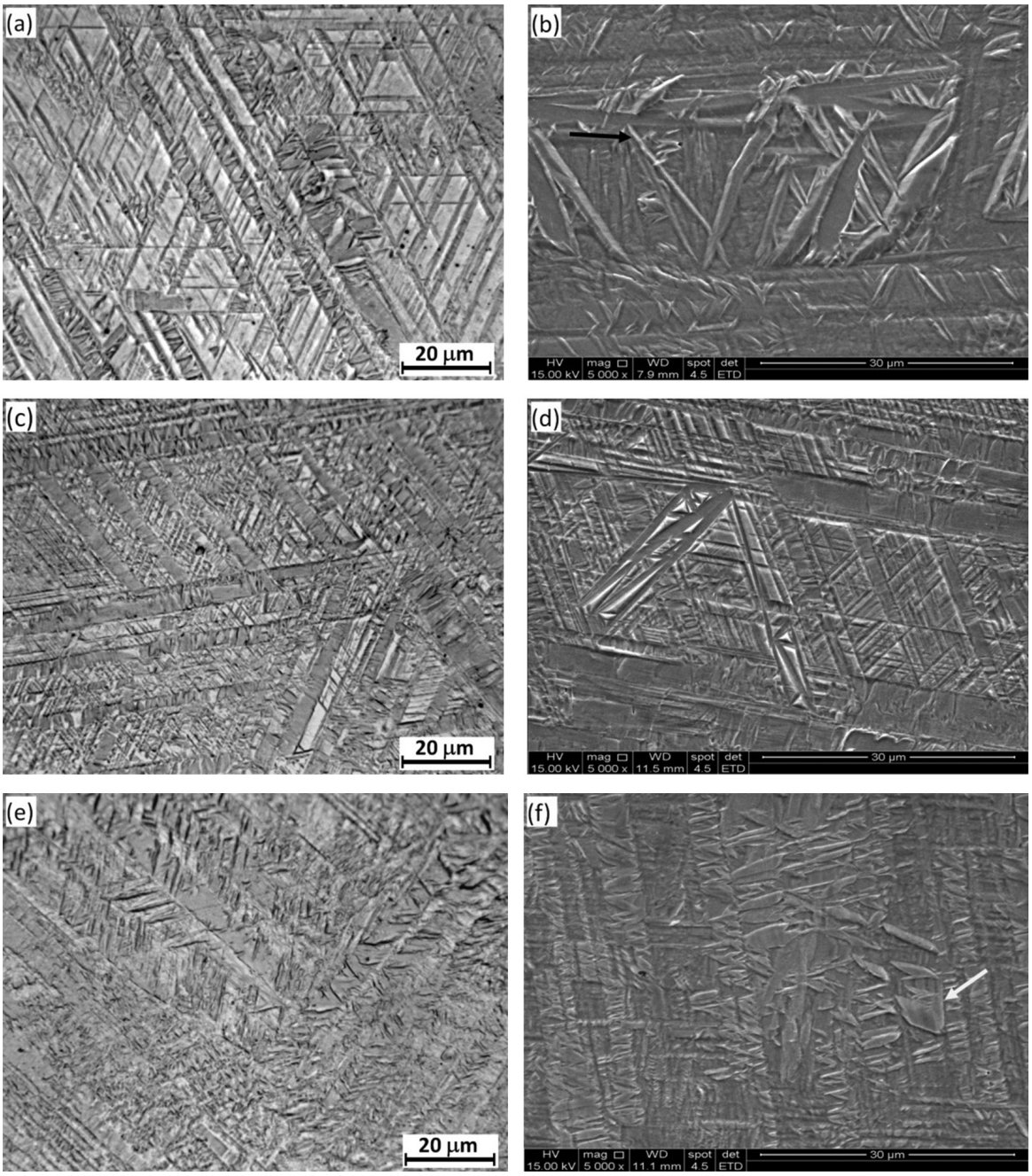

Figure 4. Optical (left) and scanning electron (right) micrographs of the samples (a, b) furnace cooled, (c, d) air cooled, and (e, f) water quenched. Samples were etched with 4% Nital.

the plates changes. The plates of ε martensite are formed by low angle laths, thus forming the packages (Figures 5a-c). It can also be observed that the formation of several packets of martensite occurs in the same grain. These packets tend to maintain an orientation of 60° (close to each other), thereby forming equilateral triangles (Figure 4c and 4d). The size of the packet is limited by its neighbors (Figures 4e and 4f).

Similarly, the growth of packages is hindered by other units. The original austenitic grain is divided in this way (Figures 5a-c). The examination of the microstructure at higher magnifications allows us to see that α' martensite forms in the ε martensite plates, as shown by the SEM images in Figures 3 and 4. Furthermore, the size of α' martensite plates varies significantly, which characterizes the process of nucleation and growth during the cooling procedure. This phenomenon was also observed by Lu et al.[17] in 0.0045C–18Mn alloy. The authors[17] called α' martensite of lenticular or chunky morphologies. In the current study, α' martensite of the same morphologies were observed, as indicated by arrows in Figures 4b and 4f,

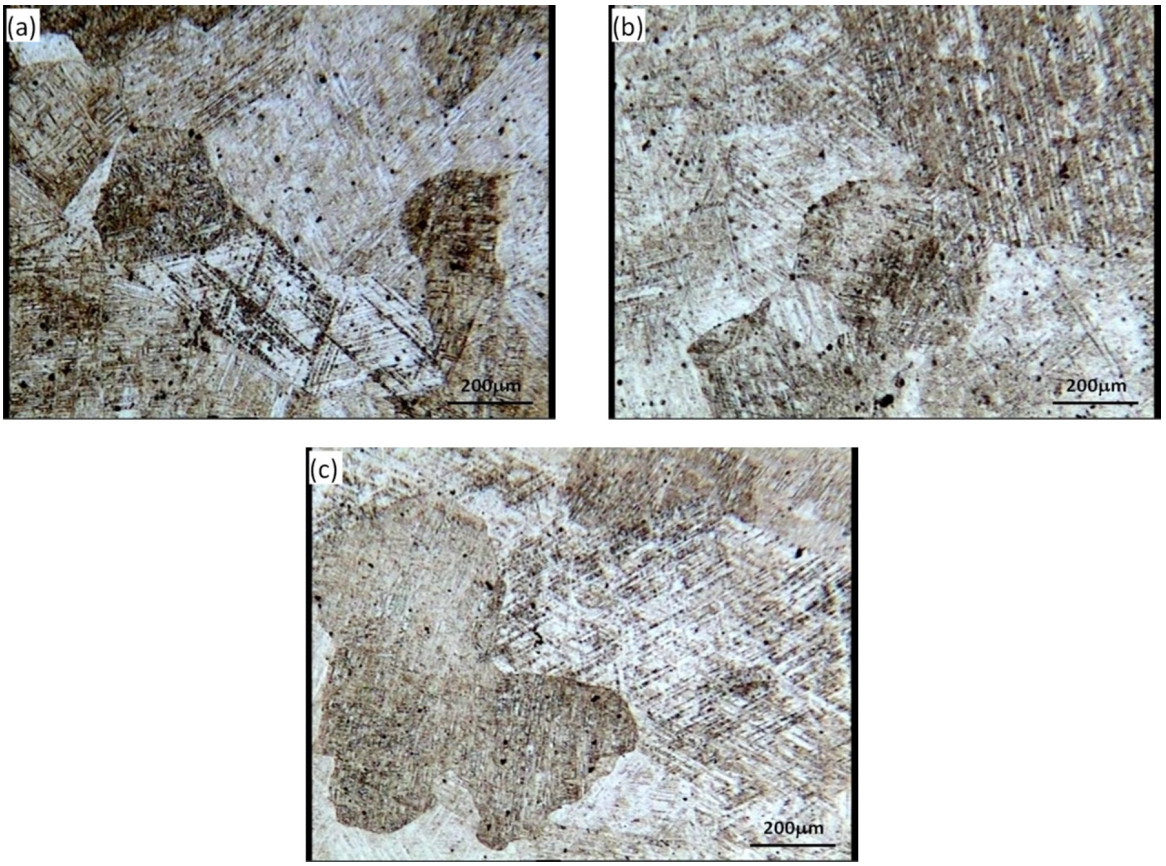

Figure 5. Optical micrographs of the samples (a) furnace cooled, (b) air cooled, and (c) water quenched. Samples were etched with 4% Nital.

respectively. The latter occurs when the martensite assumes the shape of a grain. This morphology results from a coalescence process and is possible because of the duration of the cooling process.

On the other hand, there are regions where the formation of α′ martensite is minimal and where ε martensite predominates, as shown in Figure 4d. The background regions in the micrographs correspond to the untransformed austenite. Considering this result, we can say that α′ martensite will nucleate on the g/e interface and grow into ε martensite plates through intragranular nucleation, as observed in Figures 4a and 4b.

Sahu et al.[13] analyzed the thermal stability of the as-cast homogenized austenitic steel with a basic composition of Fe–26Mn–0.14C using the Rietveld XRD pattern-fitting technique. The decomposition of austenite was observed to be very sensitive to the cooling rate. A very high proportion (49-70%) of ε martensite was found in differently cooled specimens, as well as in the as-cast specimen. The same distribution of ε martensite volume fraction was found in the present study, as seen in Table 2. According to Sahu et al.,[13] the significant variation in the extent of the $\gamma \rightarrow \varepsilon \rightarrow \alpha'$ transformation resulted from the athermal and isothermal martensites formed during cooling and the initial grain size of the austenite. Their results are in good agreement with those of the present study, in which a volume fraction of ~80% martensite was attained, despite the significant difference in steel chemical composition.

Hot-rolled structure

Figure 6 shows the optical and scanning electron micrographs of the hot-rolled sample. In the present work, the steel was cooled in air after hot rolling. Large parallel laths crossing the micrograph correspond to ε martensite, whereas α′ martensite is formed within the laths at 60° tilt angles (Figure 6b). Similar to the heat-treated samples, the size difference between the α' martensite grains is noted. The grain-boundary structures created during hot rolling provide martensite sites for nucleation. The martensite also nucleates on the stacking faults[15]. The driving force for the $\gamma \rightarrow \varepsilon$ martensite transformation remarkably increases when the steel is heated at high temperature owing to the dissolution of dislocation tangles and networks, which arises because of prior hot rolling[8]. In addition to the clean microstructure, there is grain growth with an associated reduction in the number of grain boundaries, which hinders the development of martensite. However, the austenitic grain refinement imposed by hot rolling led to a lower volume fraction of ε and α′ martensite.

In the case of large austenitic grain sizes, branching of ε martensite plates will form, allowing the continuity of the $\gamma \rightarrow \varepsilon$ transformation[11]. For fine austenitic grains, i.e., after hot rolling, the martensite plate reaches the opposite grain boundary without ε ramification. This process is interrupted, resulting in a greater volume fraction of austenite.

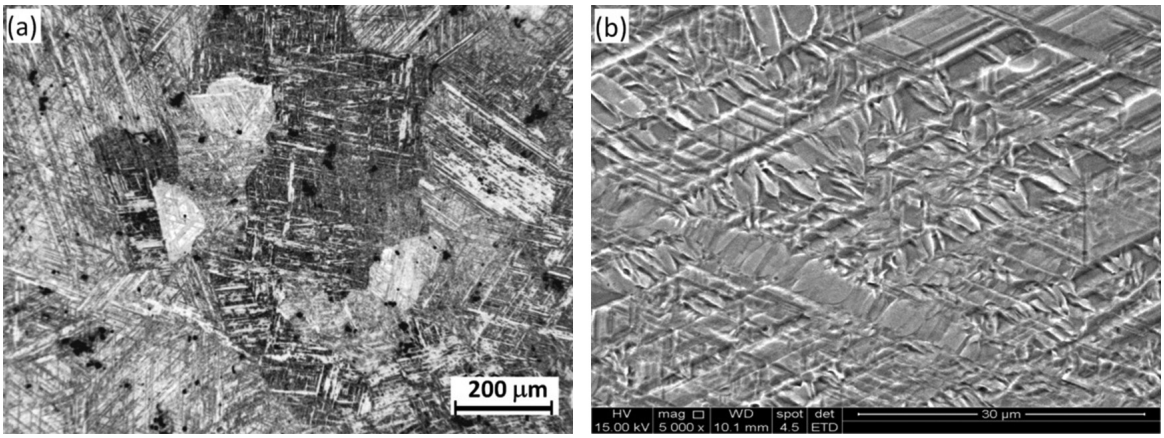

Figure 6. (a) Optical and (b) scanning electron micrographs of hot-rolled sample. Sample was etched with 4% Nital.

The austenite grain size strongly influences the martensite formation start temperature (M_s). The increase in the volume fraction of α′ martensite with increase in the austenitic grain size is associated with increase in M_s, as well as with the greater area available for transformation of austenite into martensite. SFE decreases with increasing size of the austenite grain[27,28]. In steels with low SFE, a perfect displacement in the fcc array can easily be divided into two partial dislocations, thus forming a stacking fault. Four or five layers of stacking faults are considered to be a potential nucleus for α' martensite[16]. Thus, the higher the austenitic grain size, the greater the probability of finding nucleation sites for α′ martensite, formed by superimposing stacking faults, leading to a high M_s temperature[15,29,30] and consequently, more time for transformation. All these conditions contributed to a large volume fraction of martensite formed in the steel under study, even in the absence of applied external stress and submitted to slow cooling.

Dini et al.[12] established the martensite formation in high-Mn TWIP steel. Their quantitative microstructural characterization of steel by X-ray patternfitting by the Rietveld method indicated that the volume fraction of α′ martensite increased with increasing austenite grain size. This condition is in accordance with the present results, in which large austenite grain size led to a greater volume fraction of martensite.

Hamada et al.[14] worked on a high-Mn (Fe–26Mn–0.14C) austenitic steel hot compressed at 900, 1000, and 1100 °C with a strain rate of 5 s^{-1} followed by air cooling (AC) or water quenching (WQ). The occurrence of dynamic recrystallization (DRX) produced a fine grain size (~10 mm), which was found to prevent α' and ε martensite transformation upon cooling. In the current experiment, a coarser grain size (40 mm) allowed the transformation to proceed until reaching an ε martensite volume fraction of 17%. The grain boundaries, twins, and stacking faults enhance or suppress the phase transformation,[29,30] depending on the size of the grains. For the hot-rolled samples, rolled the grain size was reduced to ~100 μm (Figure 6a), well above the critical size (10 μm[14]), thereby allowing the formation of up to 58% volume fraction of α' and ε martensite (Table 2).

In the industrial processing of this steel grade, the athermal formation of martensite has to be considered in order to obtain an adequate volume fraction of austenite at room temperature, thus making it possible to take advantage of steel workhardening and high-strength behavior. An alternative is to produce a very fine grain after cold rolling and then annealing in order to stabilize the austenite.

4. Conclusions

Both ε and α' martensite formed in the present steel after being subjected to different cooling rates, mainly in an athermal mode, assisted by some strain resulting from solidification or thermal contraction.

In the as-cast sample, despite the slow cooling, it was still possible to produce residual stress owing to contraction during the solidification of the alloy. These stresses helped to increase the formation of a larger volume fraction of α' martensite. The same reasoning applied to the sample cooled in water. In this case, there were stresses owing to thermal contraction and phase transformation. For the sample cooled in the furnace, the longer stay at high temperatures allowed to release the stress, resulting in a lower volume fraction of α' martensite, a greater volume fraction of ε martensite, and stabilization of the austenite. The sample cooled in air resulted in a larger volume fraction of ε martensite, implying that the phase-transformation kinetics are favored by a longer cooling time in relation to the cooling carried out in water.

When steel is hot rolled, its microstructure gets refined, resulting in a smaller grain size. This leads to a great volume fraction of the stabilized austenite and ε martensite, and therefore a smaller α' martensite volume fraction.

Therefore, we can conclude that the α′ martensite results from ε transformation through the mechanism $\gamma \rightarrow \varepsilon \rightarrow \alpha'$.

Acknowledgments

The authors thank the FAPEMIG, process number TEC PPM-00373/11, CNPq, process number 471128/2011-2, and the CAPES-PDSE scholarship of SSFD for the financial support to carry out this research.

References

1. Kim YG, Kim TW, Han JK and Chang RW. Development of new austenitic Fe-Mn-Al-C steels for automotive applications. *Key Engineering Materials*. 1993; 84-85:461-472. http://dx.doi.org/10.4028/www.scientific.net/KEM.84-85.461
2. Grassel O, Kruger L, Frommeyer G and Meyer LW. High strength Fe-Mn-(Al,Si) TRIP/TWIP steels development - properties - application. *International Journal of Plasticity*. 2000; 16:1391-1409. http://dx.doi.org/10.1016/S0749-6419(00)00015-2
3. Frommeyer G, Brüx U and Neumann P. Supra-ductile and high-strength manganese-TRIP/TWIP steels for high energy absorption purposes. *ISIJ International*. 2003; 43:438-446. http://dx.doi.org/10.2355/isijinternational.43.438
4. Scott C, Allain S, Faral M and Guelton N. The development of a new Fe-Mn-C austenitic steel for automotive applications. *La Revue de Métallurgie*. 2006; 6:293-302. http://dx.doi.org/10.1051/metal:2006142
5. DeCooman BC, Kwon O and Chin K-G. State-of-the-knowledge on TWIP steel. *Materials Science and Technology*. 2012; 28:513-527. http://dx.doi.org/10.1179/1743284711Y.0000000095
6. Shumann H. Die martensitischen umwandlungen in kohlenstoffarmen mangastählen. *Archiv für das Eisenhüttenwersen*. 1967; 8:647-654.
7. Sato K, Ichinose M, Hirotsu Y and Inoue Y. Effects of deformation induced phase transformation and twinning on the mechanical properties of austenitic Fe-Mn-AI alloys. *ISIJ International*. 1989; 29:868-877. http://dx.doi.org/10.2355/isijinternational.29.868
8. Jang WY, Gu Q, Van Humbeek J and Delay I. Microscopic observation of γ-phase and ε and α'- martensite in Fe-Mn-Si-based shape memory alloys. *Materials Characterization*. 1995; 34:67-72. http://dx.doi.org/10.1016/1044-5803(94)00054-O
9. Bracke L, Kestens L and Penning J. Influence of α'-martensite in an austenitic Fe-Mn-C-N alloy. *Scripta Materialia*. 2007; 57:385-388. http://dx.doi.org/10.1016/j.scriptamat.2007.05.003
10. Lu Y, Hutchinson B, Molodov DA and Gottstein G. Effect of deformation and annealing on the formation and reversion of ε-martensite in an Fe-Mn-C alloy. *Acta Materialia*. 2010; 58:3079-3090. http://dx.doi.org/10.1016/j.actamat.2010.01.045
11. Takaki S, Nakatsu H and Tokunaga Y. Effects of austenite grain size on ε martensitic transformation in Fe-15mass%Mn alloy. *Materials Transactions Online - The Japan Institute of Metals*. 1993; 34:489-495.
12. Dini G, Najafizadeh A, Monir-Vaghefi SM and Ueji R. Grain size effect on the martensite formation in a high-manganese TWIP steel by the Rietveld method. *Materials Science and Technology*. 2010; 26:181-186. http://dx.doi.org/10.1016/S1005-0302(10)60030-8
13. Sahu P, Hamada AS, Ghosh RN and Karjalainen LP. X-ray diffraction study on cooling-rate-induced $g_{fcc} \rightarrow \varepsilon_{hcp}$ martensitic transformation in cast-homogenized Fe-26Mn-0.14C austenitic steel. *Metallurgical and Materials Transactions A*. 2007; 38:1991-2000. http://dx.doi.org/10.1007/s11661-007-9240-4
14. Hamada AS, Sahu P, Chowdhury SG, Karjalainen LP, Levoska J and Oittinen T. Kinetics of the α' martensitic transformation in fine-grained Fe-26Mn-0.14C austenitic steel. *Metallurgical and Materials Transactions A*. 2008; 39:462-465. http://dx.doi.org/10.1007/s11661-007-9424-y
15. Sahu P, Hamada AS, Chowdhury SG and Karjalainen LP. Structure and microstructure evolution during martensitic transformation in wrought Fe-26Mn-0.14C austenitic steel: an effect of cooling rate. *Journal of Applied Crystallography*. 2007; 40:354-361. http://dx.doi.org/10.1107/S0021889807005882
16. Lee Y-K and Choi C-S. Driving force for $\gamma \rightarrow \varepsilon$ martensitic transformation and stacking fault energy of g in Fe-Mn binary system. *Metallurgical and Materials Transactions A*. 2000; 31:355-360. http://dx.doi.org/10.1007/s11661-000-0271-3
17. Lu F, Yang P, Meng L, Cui F and Ding H. Influences of thermal martensites and grain orientations on strain-induced martensites in high manganese TRIP/TWIP steels. *Journal of Materials Science & Technology*. 2011; 27:257-265. http://dx.doi.org/10.1016/S1005-0302(11)60059-5
18. Dumay A, Chateau J-P, Allain S, Migot S and Bouaziz O. Influence of addition elements on the stacking-fault energy and mechanical properties of an austenitic Fe-Mn-C steel. *Materials Science and Engineering:* A. 2008; 483-484:184-187. http://dx.doi.org/10.1016/j.msea.2006.12.170
19. Martin S, Ullrich C, Šimek D, Martin U and Rafaja D. Stacking fault model of ε-martensite and its DIFFaX implementation. *Journal of Applied Crystallography*. 2011; 44:779-787. http://dx.doi.org/10.1107/S0021889811019558
20. Verbeken K, Van Caenegem N and Raabe D. Identification of ε martensite in a Fe-based shape memory alloy by means of EBSD. *Micron.* 2009; 40:151-156. http://dx.doi.org/10.1016/j.micron.2007.12.012
21. Ding H, Tang Z-Y, Li W, Wang M and Song D. Microstructures and mechanical properties of Fe-Mn-(Al-Si) TRIP/TWIP Steels. *Journal of Iron and Steel Research International*. 2006; 13:66-70. http://dx.doi.org/10.1016/S1006-706X(06)60113-1
22. Sugimoto K, Usui N, Kobayashi M and Hashimoto S. Effects of volume fraction and stability of retained austenite on ductility of TRIP-aided dual-phase steels. *ISIJ International*. 1992; 32:1311-1318. http://dx.doi.org/10.2355/isijinternational.32.1311
23. Olson GB and Cohen M. A general mechanism of martensitic nucleation: Part I. general concepts and the FCC→HCP transformation. *Metallurgical Transactions A*. 1976; 7:1897-1904. http://dx.doi.org/10.1007/BF02654987
24. Yang H-S, Jang JH, Bhadeshia HKDH and Suh DW. Critical assessment: Martensite-start temperature for the $\gamma \rightarrow \varepsilon$ transformation. *CALPHAD:* Computer Coupling of Phase Diagrams and Thermochemistry 2012; 36:16-22. http://dx.doi.org/10.1016/j.calphad.2011.10.008
25. Tsuzaki K,Fukasaku S, Tomota Y and Maki T. Effect of prior Deformation of Austenite on the $\gamma \rightarrow \varepsilon$ martensitic Transformation in Fe-Mn Alloys. JIM. 1991; 32:222-228.
26. Suh D-W, Park S-J, Lee C-H and Kim S-J. Microstructure and mechanical behaviors of 0.1C-13Mn metastable austenitic steel. *Metallurgical and Materials Transactions A*. 2009; 40:264-267. http://dx.doi.org/10.1007/s11661-008-9734-8
27. Naraghi R, Hedström P and Borgenstam A. Spontaneous and deformation-induced martensite in austenitic stainless steels with different stability. *Steel Research International*. 2011; 82:337-345. http://dx.doi.org/10.1002/srin.201000118
28. Jun J-H and Choi C-S. Variation of stacking fault energy with austenitic grain size and its affect on the M_s temperature of $\gamma \rightarrow \varepsilon$ martensitic transformation in Fe-Mn alloy. *Materials Science and Engineering:* A. 1998; 257:353-356. http://dx.doi.org/10.1016/j.jallcom.2006.09.044
29. Güler E, Kirindi T and Aktas H. Comparison of thermally induced and deformation induced martensite in Fe-29%Ni-2%Mn alloy. *Journal of Alloys and Compounds*. 2007; 440:168-172. http://dx.doi.org/10.1016/j.jallcom.2006.09.044
30. Liang X, Wang X and Zurob HS. Microstructural characterization of transformable Fe-Mn alloys at different length scales. *Materials Characterization*. 2009; 60:1224-1231. http://dx.doi.org/10.1016/j.matchar.2009.04.015